DAMAGE ASSESSMENT AND DISASTER PREVENTION IN NATM TUNNELS DURING CONSTRUCTION: MICROMECHANICS-SUPPORTED HYBRID ANALYSES

H.A. Mang (herbert.mang@tuwien.ac.at), S. Scheiner,
B. Pichler, and C. Hellmich
Institute for Mechanics of Materials and Structures, Vienna University of Technology, Karlsplatz 13, 1040 Vienna, Austria

Abstract. Knowledge of the stresses in shotcrete tunnel shells is of great importance for assessing their safety against severe cracking or failure. Estimation of these stresses from 3D optical displacement measurements requires shotcrete material models allowing for variation of the water–cement and the aggregate–cement ratio. This is the motivation for employing two representative volume elements within a continuum micromechanics framework: One of them relates to cement paste (with a spherical material phase representing clinker, needle-shaped hydrate phases with isotropically distributed spatial orientations, a spherical water phase, and a spherical air phase, with all phases being in mutual contact), whereas the second one relates to shotcrete (with phases representing cement paste and aggregates, whereby aggregate inclusions are embedded into a matrix made up by cement paste). Elasticity homogenization follows self-consistent schemes (at the cement paste level) and Mori–Tanaka estimates (at the shotcrete level). Stress peaks in the hydrates related to quasi-brittle material failure are estimated by second-order phase averages derived from the RVE-related elastic energy. The latter permits upscaling from the hydrate strength to the shotcrete strength. Experimental data from resonant frequency tests, ultrasonics tests, adiabatic tests, uniaxial compression tests, and nanoindentation tests suggest that early-age (evolving) shotcrete elasticity and strength can be reasonably well predicted from mixture- and hydration-independent mechanical properties of aggregates, clinker, hydrates, water, and air, and from the strength properties of the hydrates. Notably, the model-predicted final strength (at completed hydration) almost perfectly follows the famous Feret formula. At the structural level, the micromechanics model, when combined with 3D displacement measurements, predicts that a decrease of the water–cement ratio increases the safety of the shotcrete tunnel shell whereas standard-type variations in the aggregate–cement ratio, because of rebound during shotcreting, have virtually no influence on the overall structural safety.

Keywords: Micromechanics, shotcrete, hydration, elasticity, strength, tunneling, New Austrian tunneling method

A. Ibrahimbegovic and M. Zlatar (eds.), *Damage Assessment and Reconstruction After War or Natural Disaster*,

1. Introduction

Disasters resulting from damage and failure of civil engineering structures, caused either by short-term influences (earthquake ground motion, explosions, or fires) or by long-term loadings (corrosion, wear, pollution) may occur during service as well as in the construction process itself, in particular, if construction leads to significant changes of the original conditions. This is particularly true for the field of underground tunneling where complicated ground conditions often call for sophisticated methods such as the so-called New Austrian Tunneling Method (NATM) (Rabcewicz 1948, 1964a, b,1965; Karakuş and Fowell, 2004). While being extremely successful in cases where a high degree of flexibility is required, use of this method is also related to what was called 'Britain's worst civil engineering disaster in modern times' (Bishop, 1994), namely, to a series of collapses of thin support shells (Oliver, 1994) during the construction of the Heathrow express station tunnel at London's busiest airport. Installation of such thin support shells or primary linings right after excavation of a small stretch of a tunnel is one of the key elements of the NATM, apart from utilization of the ground surrounding the tunnel as structural element (which may also be reinforced by rock bolts) and from final stabilization of the tunnel by a secondary lining. Since failure of the primary lining is one of the major causes for the disasters that were encountered during NATM tunnel construction, great efforts have been undertaken to monitor the behavior of the freshly installed lining. As of today, 3D optical monitoring systems (Steindorfer et al., 1995; Schubert and Steindorfer, 1996) are the golden standard. Changes of characteristic trend parameters, extracted from 3D displacement measurements, allow to estimate changes in the geological structure of the soil or rock (Schubert et al., 2002).

Understanding of the mechanics of NATM tunnel shells has turned out to be the key to safety increase and disaster prevention in modern NATM tunneling. For almost 2 decades, this was the driving force for theoretical, experimental, and computational mechanics research at the Institute for Mechanics of Materials and Structures (IMWS) of Vienna University of Technology. The present book chapter reviews the Institute's latest achievements in safety assessment and disaster prevention of thin primary support shells, based on an integrated analysis method which combines monitoring data with advanced multiscale mechanics concepts, directly integrating concrete composition and chemical information related to so-called performance-based shotcrete tunnel design. In more detail, the strains in the shotcrete tunnel shell are obtained from the aforementioned 3D optical displacement vector measurements, as proposed by Rokahr and Zachow (1997) on the basis of relative movements of pairs of measurement points. At the IMWS, this conceptual approach was further elaborated: The strain *fields* can be estimated on the basis of a hybrid method (Hellmich, 1999; Hellmich et al., 1999a, 2001), in which displacement vector fields are approximated through interpolation of measured displacement vectors at discrete points of the tunnel shell. These fields are then prescribed as boundary values for a three-dimensional Finite Element structural model of the tunnel shell. This method was extended to segmented tunnel linings (Macht et al., 2000; Lackner et al., 2002); use of approximations from thin shell theory (Macht et al., 2003; Lackner et al., 2006) turned out to be beneficial for day-to-day use of the hybrid method in engineering practice (Brandtner et al., 2007).

The underlying shotcrete models must represent the creep behavior of the material (Rokahr and Lux, 1987; Schubert, 1988; Lechner et al., 2001) reasonably well. Consideration of hydration-induced, thermal and chemical strains further improves the reliability of estimations of the internal forces of the shell (Hellmich et al., 1999b, c; Sercombe et al., 2000 Lechner et al., 2001). All aforementioned material models rely on shotcrete mixture-specific material properties. Hence, any change in mixture (e.g. a variation of the water–cement ratio, as often encountered *in situ*) can only be considered if additional experiments (related to strength, creep, and shrinkage) are performed on samples with the modified concrete composition. This is often unfeasible so that engineers on site frequently agree on a 'typical' shotcrete for a tunnel track.

Clearly, this situation is unsatisfactory. As a remedy, the shotcrete composition (in terms of the water–cement ratio w/c and the aggregate–cement ratio a/c) needs to be incorporated into the shotcrete material models, within a micromechanical framework: This was recently shown by Hellmich and Mang (2005) for the case of elasticity – following earlier work on concrete by Bernard et al. (2003) and on bone by Hellmich and Ulm (2002). While stiffness is an important factor for attracting stresses to the tunnel shell, strength is the key factor to understand whether these stresses significantly compromise the shell's safety. Also the evolution of strength is influenced by the w/c- and the a/c-ratio (Neville, 1981). Here we review a first micromechanical model for shotcrete elasticity and strength (Pichler et al. 2008a, b). By way of example, we employ this new model to hybrid analysis of a NATM tunnel shell. Extending results published earlier (Pichler et al., 2008b), we not only study the influence of the water–cement ratio on the safety level of the thin primary lining but also the one of the aggregate–cement ratio which typically fluctuates because of varying rebound of aggregates during shotcreting.

The book chapter is organized as follows: After a short review of the fundamentals of continuum micromechanics (Section 2), upscaling of stiffness and strength properties (Sections 3 and 4) from the hydrate level, via the cement paste level, to the shotcrete level is described. This is followed by experimental validation (Section 5) of the new micromechanics model and by its application to a NATM-tunnel safety assessment (Sections 6 and 7).

2. Fundamentals of micromechanics – representative volume element (RVE)

In continuum micromechanics (Hill, 1963; Suquet, 1997; Zaoui, 1997, 2002), a material is understood as a macro-homogeneous but micro-heterogeneous body filling a representative volume element (RVE) with characteristic length ℓ, $\ell \gg d$, d standing for the characteristic length of inhomogeneities within the RVE, and $\ell \ll \mathcal{L}$, $\mathcal{L}$ standing for the characteristic lengths of geometry or loading of a structure built up by the material defined on the RVE. In general, the microstructure within an RVE is too complicated to describe it in full detail. Therefore, quasi-homogeneous subdomains with known physical quantities (such as volume fractions or elastic properties) are reasonably chosen. They are called material phases. The 'homogenized' mechanical behavior of the overall material, i.e., the relation between homogeneous deformations acting on the boundary of the RVE and resulting (average) stresses, or the ultimate stresses sustainable by the RVE, can then be estimated from the mechanical behavior of the aforementioned homogeneous phases (representing the inhomogeneities within the RVE), their dosages within the RVE, their characteristic shapes, and their interactions. If a single phase exhibits a heterogeneous microstructure itself, its mechanical behavior can be estimated by introduction of an RVE within this phase, with dimensions $\ell_2 \leq d$, comprising again smaller phases with characteristic length $d_2 \ll \ell_2$, and so on, leading to a multistep homogenization scheme.

For shotcrete, we employ two RVEs: The first one relates to cement paste (with phases representing clinker, water, hydrates, and air), and the second one to shotcrete (with phases representing cement paste and aggregates), see Fig. 1.

3. Micromechanics at the cement paste level

3.1. MICROMECHANICAL REPRESENTATION

We consider an RVE$_{cp}$ of cement paste with characteristic length $\ell_{cp} =$ 0.25–0.50 mm, see Fig. 1a, consisting of four different material phases with characteristic dimensions $d_{cp} = 1{-}50\,\mu$m (see also Fig. 2): (i) a spherical clinker phase, (ii) needle-shaped hydrate phases with isotropically

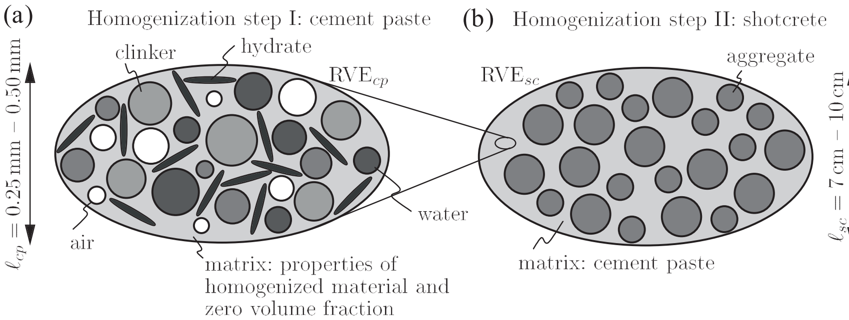

Figure 1. Micromechanical representation of shotcrete microstructure through a two-step homogenization scheme: 2D sketches of 3D representative volume elements (RVEs) – (**a**) the polycrystalline RVE of 'cement paste', RVE$_{cp}$, is built up of clinker, water, needle-shaped hydrates, and air; (**b**) the RVE of the matrix-inclusion composite 'shotcrete', RVE$_{sc}$, is composed of a cement paste matrix with aggregate inclusions

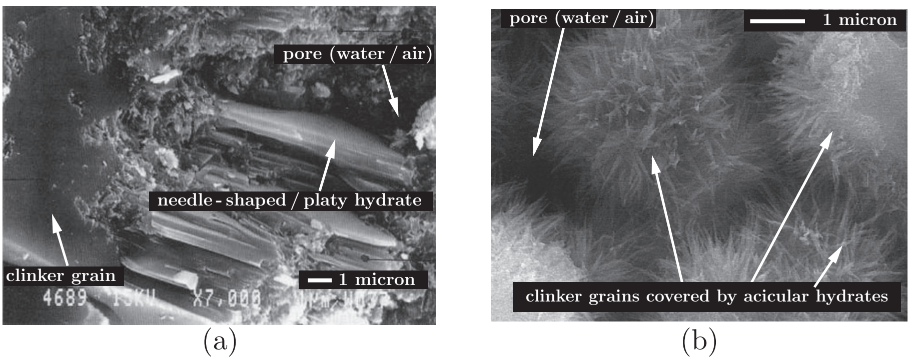

Figure 2. Images of cement paste obtained by Scanning Electron Microscopy showing non-spherical hydrates: (**a**) from Baroghel-Bouny (1994), (**b**) from Tritthart and Häußler (2003)

distributed spatial orientations, (iii) a spherical water phase, and (iv) a spherical air phase.

Macroscopic strains $\mathbf{E}_{cp}$ are imposed at the boundary of the RVE$_{cp}$ in terms of displacement vectors $\boldsymbol{\xi}$ (Hashin, 1983),

$$\text{on } \partial\Omega_{cp} : \boldsymbol{\xi}(\mathbf{x}) = \mathbf{E}_{cp} \cdot \mathbf{x}\,, \tag{1}$$

with $\mathbf{x}$ as the position vector within the RVE$_{cp}$. The geometrical compatibility of (1) with the local microscopic strains $\boldsymbol{\varepsilon}(\mathbf{x})$ within the RVE$_{cp}$ implies

$$\mathbf{E}_{cp} = \frac{1}{\Omega_{cp}} \int_{\Omega_{cp}} \boldsymbol{\varepsilon}(\mathbf{x})\, dV = \sum_p f_p\, \boldsymbol{\varepsilon}_p\,, \tag{2}$$

with $p = clin, H_2O, hyd, air$, Ω_{cp} as the volume of the RVE_{cp}, f_{clin}, f_{H_2O}, f_{hyd}, and f_{air} as the volume fractions of clinker, of water, of hydrates, and of air, respectively, and with

$$\boldsymbol{\varepsilon}_p = \frac{1}{\Omega_p} \int\limits_{\Omega_p} \boldsymbol{\varepsilon}(\mathbf{x}) \, \mathrm{d}V \,, \tag{3}$$

as the first-order (spatial average) phase strains. Considering the needle shape of the hydrate phases, the strain average rule (2) takes the form

$$\mathbf{E}_{cp} = \sum_p f_p \, \boldsymbol{\varepsilon}_p + f_{hyd} \int\limits_{\varphi=0}^{2\pi} \int\limits_{\vartheta=0}^{\pi} \boldsymbol{\varepsilon}_{hyd;\varphi,\vartheta} \frac{\sin\vartheta}{4\pi} \, \mathrm{d}\vartheta \, \mathrm{d}\varphi \,. \tag{4}$$

with $p = clin, H_2O, air$, and with the Euler angles φ and ϑ defining the orientations of the hydrate needles, see Pichler et al. (2008b) for details. The average strains in the hydrate needles, $\boldsymbol{\varepsilon}_{hyd;\varphi,\vartheta}$, are defined through

$$\boldsymbol{\varepsilon}_{hyd;\varphi,\vartheta} = \lim_{\Delta\varphi,\Delta\vartheta \to 0} \left(\frac{1}{\Omega_{hyd;\varphi,\vartheta}} \int\limits_{\Omega_{hyd;\varphi,\vartheta}} \boldsymbol{\varepsilon}(\mathbf{x}) \, \mathrm{d}V \right) , \tag{5}$$

By analogy to (2), the macroscopic stresses $\boldsymbol{\Sigma}_{cp}$ are equal to the spatial average of the (equilibrated) local stresses $\boldsymbol{\sigma}(\mathbf{x})$ inside the RVE_{cp},

$$\boldsymbol{\Sigma}_{cp} = \frac{1}{\Omega_{cp}} \int\limits_{\Omega_{cp}} \boldsymbol{\sigma}(\mathbf{x}) \, \mathrm{d}V = \sum_p f_p \, \boldsymbol{\sigma}_p + f_{hyd} \int\limits_{\varphi=0}^{2\pi} \int\limits_{\vartheta=0}^{\pi} \boldsymbol{\sigma}_{hyd;\varphi,\vartheta} \frac{\sin\vartheta}{4\pi} \, \mathrm{d}\vartheta \, \mathrm{d}\varphi \,, \tag{6}$$

with $p = clin, H_2O, air$, and with phase stresses $\boldsymbol{\sigma}_p$ and $\boldsymbol{\sigma}_{hyd;\varphi,\vartheta}$ defined analogously to the aforementioned phase strains $\boldsymbol{\varepsilon}_p$ and $\boldsymbol{\varepsilon}_{hyd;\varphi,\vartheta}$, see (3) and (5).

3.2. CONSTITUTIVE BEHAVIOR OF CLINKER, WATER, HYDRATES, AND AIR

We assign linear elastic behavior to all phases, i.e.

$$\boldsymbol{\sigma}_p = \mathbf{C}_p : \boldsymbol{\varepsilon}_p \,, \tag{7}$$

with $\mathbf{C}_p$ as the fourth-order stiffness tensor of phase p, $p = clin, H_2O, hyd, air$. Assuming isotropy for all phases, $\mathbf{C}_p$ reads as

$$\mathbf{C}_p = 3k_p\mathbf{J} + 2\mu_p\mathbf{K} \,, \tag{8}$$

whereby $\mathbf{K}$ is the deviatoric part of the fourth-order unit tensor, defined as $\mathbf{K} = \mathbf{I} - \mathbf{J}$, with $\mathbf{I}$ as the symmetric fourth-order unit tensor with components $I_{ijrs} = 1/2(\delta_{ir}\delta_{js} + \delta_{is}\delta_{jr})$, and with $\mathbf{J} = 1/3(\mathbf{1} \otimes \mathbf{1})$ as the volumetric part of the fourth-order unit tensor, where $\mathbf{1}$ denotes the second-order unit tensor with components δ_{ij} (Kronecker delta), $\delta_{ij} = 1$ for $i = j$, and $\delta_{ij} = 0$ otherwise. The phase stiffnesses $\mathbf{C}_p$, in terms of the bulk modulus k_p and the shear modulus μ_p, are available from experiments (see Table 1): Hydrate stiffnesses follow from nanoindentation experiments (Acker, 2001; Constantinides and Ulm, 2004); we here consider the elastic properties of low-density calcium silicate hydrates (C-S-H) as representative for all hydrates, see also Hellmich and Mang (2005) for details. Clinker properties are taken from Acker (2001). If, upon loading, no water can escape from the RVE_{cp} (sealed or undrained conditions), we consider an elastic water phase with negligible shear stiffness as a very good approximation of 'undrained conditions in the sense of a fully *poro*-micromechanical theory' (Hellmich and Ulm, 2005), whereas a zero water stiffness relates to drained conditions. The zero-stiffness air phase is also in a 'drained' state.

TABLE 1. Intrinsic mechanical properties of microstructural constituents of shotcrete

Phase	Bulk modulus k [GPa]	Shear modulus μ [GPa]	Reference
Clinker	$k_{clin} = 116.7$	$\mu_{clin} = 53.8$	Acker (2001)
Water (drained RVE)	$k_{H_2O} = 0.0$	$\mu_{H_2O} = 0.0$	
Water (sealed RVE)	$k_{H_2O} = 2.3$	$\mu_{H_2O} = 0.0$	
Hydrates	$k_{hyd} = 14.1$	$\mu_{hyd} = 8.9$	Ulm et al. (2004)
Air	$k_{air} = 0.0$	$\mu_{air} = 0.0$	
Aggregate	$k_{agg} = 41.7$	$\mu_{agg} = 19.2$	Wesche (1974), Mehlhorn (1996)

Uniaxial compression tests on cement paste (or shotcrete) samples reveal linear elastic behavior until, close to the compressive strength, axial strains increase overlinearly with increasing axial stresses. Once the peak load is reached, the material exhibits quasi-brittle failure. Hence, the strength of cement paste (or of shotcrete) can be estimated by means of elastic limit analysis (Pichler et al., 2008a). Moreover, it is assumed that the elastic limits of the hydrates govern the elastic limits of cement paste and of the shotcrete. I.e. each hydrate behaves linearly elastic as long as microscopic deviatoric stress peaks remain below a specific critical value. If, because of a (compressible uniaxial) macroscopic load increase, this critical value is reached in the most strongly stressed region of the hydrate phase, the elastic limit on the microscale is reached, which, in turn, corresponds to the macroscopic elastic limit of cement paste (or shotcrete), associated with failure of the material (under macroscopic uniaxial compression). In more detail, load bearing capacities of the hydrates are being bounded according to a *von Mises*-type elastic limit criterion (Pichler et al., 2008a),

$$\max_{\mathbf{x}\in\Omega_{hyd}} \sigma^{dev}(\mathbf{x}) = \max_{\mathbf{x}\in\Omega_{hyd}} \left[\left(\frac{1}{2}\,\boldsymbol{\sigma}^{dev}(\mathbf{x}) : \boldsymbol{\sigma}^{dev}(\mathbf{x})\right)^{\frac{1}{2}}\right] \leq \sigma^{dev}_{crit}\,, \tag{9}$$

where $\sigma^{dev}(\mathbf{x})$ is the norm of stress deviator $\boldsymbol{\sigma}^{dev}(\mathbf{x})$ defined by

$$\boldsymbol{\sigma}^{dev}(\mathbf{x}) = \mathbf{K} : \boldsymbol{\sigma}(\mathbf{x})\,. \tag{10}$$

The choice of hydrates as weakest locations inside the RVE_{cp} of cement paste was corroborated by Pichler et al. (2008a) who showed that the single strength-type value for $\sigma^{dev}_{crit} = 26\,\text{MPa}$ allows for prediction of uniaxial cube compressive strength of different cement pastes with w/c ranging from 0.35–0.60 (Boumiz et al., 1996; Sun et al., 2005), at different degrees of hydration ξ.

3.3. HOMOGENIZED ELASTICITY OF CEMENT PASTE

As long as the material phases behave elastically, the relation between $\mathbf{\Sigma}_{cp}$ and $\mathbf{E}_{cp}$ reads, analogous to (7), as

$$\mathbf{\Sigma}_{cp} = \mathbf{C}_{cp} : \mathbf{E}_{cp}\,, \tag{11}$$

with the 'macroscopic' homogenized stiffness tensor of cement paste, $\mathbf{C}_{cp} = 3k_{cp}\mathbf{J} + 2\mu_{cp}\mathbf{K}$, and where k_{cp} is the bulk modulus and μ_{cp} is the shear modulus. Following the traditional approach in continuum micromechanics (Zaoui, 2002), the dependence of $\mathbf{C}_{cp}$ on the phase stiffness properties (Table 1) will be established on the basis of Eshelby-Laws-type matrix-inclusion problems which are formulated separately for each phase $p = clin, H_2O, hyd, air$. The respective phase is represented by a single ellipsoidal inclusion which is embedded in an infinite matrix with stiffness $\mathbf{C}^0$, subjected to homogeneous strains $\mathbf{E}^\infty$ at infinity. This loading provokes homogeneous strains in the ellipsoidal inclusions which are of the form (Eshelby, 1957; Laws, 1977; Zaoui, 2002)

$$\boldsymbol{\varepsilon}_p = \left[\mathbf{I} + \mathbf{P}^0_p \,:\, (\mathbf{C}_p - \mathbf{C}^0)\right]^{-1} : \mathbf{E}^\infty\,. \tag{12}$$

Thereby, the Hill tensors $\mathbf{P}^0_p$ account for the shape of inclusion (phase) p in a matrix of (isotropic) stiffness $\mathbf{C}^0 = 3k^0\mathbf{J} + 2\mu^0\mathbf{K}$.

Evaluation of (12) for all phases within RVE_{cp} and insertion of the corresponding result into condition (4) yields a relation between RVE_{cp}-related strains $\mathbf{E}_{cp}$ and matrix-related strains $\mathbf{E}^{\infty}$,

$$\begin{aligned}\mathbf{E}^{\infty} \;=\; \mathbf{E}_{cp} : \Bigg\{ \sum_p f_p \left[\mathbf{I} + \mathbf{P}^0_{sph} : (\mathbf{C}_p - \mathbf{C}^0)\right]^{-1} + \\ + f_{hyd} \int\limits_{\varphi=0}^{2\pi} \int\limits_{\vartheta=0}^{\pi} \left[\mathbf{I} + \mathbf{P}^0_{cyl}(\varphi,\vartheta) : (\mathbf{C}_{hyd} - \mathbf{C}^0)\right]^{-1} \frac{\sin\vartheta}{4\pi}\, d\vartheta\, d\varphi \Bigg\}^{-1}\end{aligned} \tag{13}$$

with $p = clin, H_2O, air$. The computation of the Hill tensors for spherical material phases, $\mathbf{P}^0_{sph}$, and for cylindrical material phases, $\mathbf{P}^0_{cyl}(\varphi,\vartheta)$, respectively, is presented in detail in Pichler et al. (2008b). $\mathbf{C}^0$ in (13) is chosen according to the interaction of the phases within the RVE_{cp} (Zaoui, 2002). Since they are largely disordered and in contact with each other, we choose $\mathbf{C}^0 = \mathbf{C}_{cp}$ (self-consistent scheme [Hershey, 1954; Kröner, 1958]), and identify the homogenized stiffness of cement paste, $\mathbf{C}_{cp}$, by inserting (13) into (12), multiplying the corresponding result by $\mathbf{C}_p$, according to the phase elasticity law (7), and inserting the result of the latter operations into the stress average condition (6). Comparison of the final result with (11) yields the desired homogenized stiffness of cement paste as

$$\begin{aligned}\mathbf{C}_{cp} = \;& \Bigg\{ \sum_p f_p \mathbf{C}_p : \left[\mathbf{I} + \mathbf{P}^{cp}_{sph} : (\mathbf{C}_p - \mathbf{C}_{cp})\right]^{-1} + f_{hyd}\mathbf{C}_{hyd} : \\ & : \int\limits_{\varphi=0}^{2\pi} \int\limits_{\vartheta=0}^{\pi} \left[\mathbf{I} + \mathbf{P}^{cp}_{cyl}(\varphi,\vartheta) : (\mathbf{C}_{hyd} - \mathbf{C}_{cp})\right]^{-1} \frac{\sin\vartheta}{4\pi}\, \mathrm{d}\vartheta\, \mathrm{d}\varphi \Bigg\} : \\ & : \Bigg\{ \sum_p f_p \left[\mathbf{I} + \mathbf{P}^{cp}_{sph} : (\mathbf{C}_p - \mathbf{C}_{cp})\right]^{-1} + f_{hyd} \int\limits_{\varphi=0}^{2\pi} \int\limits_{\vartheta=0}^{\pi} \Big[\mathbf{I} + \mathbf{P}^{cp}_{cyl}(\varphi,\vartheta) : \\ & (\mathbf{C}_{hyd} - \mathbf{C}_{cp})\Big]^{-1} \frac{\sin\vartheta}{4\pi}\, \mathrm{d}\vartheta\, \mathrm{d}\varphi \Bigg\}^{-1},\end{aligned} \tag{14}$$

where $p = clin, H_2O, air$. For detailed explanations regarding the numerical evaluation of (14), see Pichler et al. (2008a, b).

3.4. HOMOGENIZED STRENGTH OF CEMENT PASTE

From loading $\mathbf{E}_{cp}$ (or $\mathbf{\Sigma}_{cp}$) of an RVE_{cp} of cement paste, we are left with estimating the stress peaks $\max \sigma^{dev}_{hyd}(\mathbf{x})$ in the hydrates relevant to the quasi-brittle failure criterion (9). We have resolved the hydrate phase Ω_{hyd} down to bundles $\Omega_{hyd;\varphi,\vartheta}$ around angles φ and ϑ. Hence, we may specify

$$\max_{\mathbf{x}\in\Omega_{hyd}} \sigma^{dev}(\mathbf{x}) = \max_{\substack{\mathbf{x}\in\Omega_{hyd;\varphi,\vartheta}\\ \varphi\in[0,2\pi]\\ \vartheta\in[0,\pi]}} \sigma^{dev}(\mathbf{x},\varphi,\vartheta)\,. \tag{15}$$

Still, in the maximally stressed bundle, not the (first-order) average phase stresses $\boldsymbol{\sigma}_{hyd;\varphi,\vartheta}$, but stress *peaks* govern the failure of the (φ,ϑ)-oriented hydrate phase (Pichler et al., 2008a). Such peaks can be estimated appropriately through quadratic stress averages over suitably chosen subdomains of the RVE$_{cp}$, such as 3D subdomains (bulk phases) (Lemarchand et al., 2002; Barthélémy and Dormieux, 2003; Hofstetter et al., 2005) or 2D interfaces (Dormieux et al., 2007; Fritsch et al., 2007). Herein we introduce quadratic (or second-order) deviatoric stress and strain averages over (φ,ϑ)-oriented hydrates, $\overline{\overline{\sigma^{dev}_{hyd;\varphi,\vartheta}}}$ and $\overline{\overline{\epsilon^{dev}_{hyd;\varphi,\vartheta}}}$, averaged, in the sense of (5), over all hydrates oriented in one direction (φ,ϑ),

$$\begin{aligned}\max_{\mathbf{x}\in\Omega_{hyd;\varphi,\vartheta}} \sigma^{dev}(\mathbf{x},\varphi,\vartheta) \;&\approx\; \overline{\overline{\sigma^{dev}_{hyd;\varphi,\vartheta}}} = \\ &= \lim\nolimits_{\Delta\varphi,\Delta\vartheta\to 0}\left(\tfrac{1}{\Omega_{hyd;\varphi,\vartheta}}\int_{\Omega_{hyd;\varphi,\vartheta}}\left[\sigma^{dev}(\mathbf{x},\varphi,\vartheta)\right]^2\,\mathrm{d}V\right)^{\frac{1}{2}}\,,\end{aligned} \tag{16}$$

so that, according to (15),

$$\max_{\mathbf{x}\in\Omega_{hyd}} \sigma^{dev}(\mathbf{x}) = \max_{\substack{\varphi\in[0,2\pi]\\ \vartheta\in[0,\pi]}} \overline{\overline{\sigma^{dev}_{hyd;\varphi,\vartheta}}}\,. \tag{17}$$

$\overline{\overline{\sigma^{dev}_{hyd;\varphi,\vartheta}}}$ can be related to macroscopic stresses $\boldsymbol{\Sigma}_{cp}$ imposed (in terms of strains $\mathbf{E}_{cp} = \mathbf{C}_{cp}^{-1} : \boldsymbol{\Sigma}_{cp}$) onto the RVE$_{cp}$ of cement paste by means of elastic energy considerations similar to those proposed by Dormieux et al. (2002), Kreher and Molinari (1993), Kreher (1990), yielding

$$\overline{\overline{\sigma^{dev}_{hyd;\varphi,\vartheta}}} = \lim_{\Delta\varphi,\Delta\vartheta\to 0}\left(-\frac{\mu^2_{hyd}}{f_{hyd;\varphi,\vartheta}}\boldsymbol{\Sigma}_{cp} : \frac{\partial\mathbf{C}^{-1}_{cp}}{\partial\mu_{hyd;\varphi,\vartheta}} : \boldsymbol{\Sigma}_{cp}\right)^{\frac{1}{2}}\,. \tag{18}$$

Setting

$$\max_{\varphi,\vartheta}\overline{\overline{\sigma^{dev}_{hyd;\varphi,\vartheta}}} = \sigma^{dev}_{crit} = 26\,\mathrm{MPa} \tag{19}$$

according to (9), (16), and (18), elastic limits of the hydrates are related to quasi-brittle failure of shotcrete which may be represented by the uniaxial compressive strength $\Sigma_{cp,11}^{comp,ult}$: The latter follows from insertion of (19) into (18), and evaluation of (18) for $\Sigma_{cp} = -\left|\Sigma_{cp,11}^{comp,ult}\right| (\mathbf{e}_z \otimes \mathbf{e}_z)$,

$$\Sigma_{cp,11}^{comp,ult} = \left\{ \max_{\varphi,\vartheta} \left[\lim_{\Delta\varphi,\Delta\vartheta\to 0} \left(- \frac{\mu_{hyd}^2}{f_{hyd;\varphi,\vartheta}} (\mathbf{e}_z \otimes \mathbf{e}_z) : \frac{\partial \mathbf{C}_{cp}^{-1}}{\partial \mu_{hyd;\varphi,\vartheta}} : : (\mathbf{e}_z \otimes \mathbf{e}_z) \right)^{\frac{1}{2}} \right] \right\}^{-1} \times \sigma_{crit}^{dev} . \tag{20}$$

An algorithm for computation of the aforementioned limit, $\lim\limits_{\Delta\varphi,\Delta\vartheta\to 0}$, is presented in Pichler et al. (2008a).

4. Micromechanics at the shotcrete level

We consider an RVE$_{sc}$ of shotcrete with the characteristic length ℓ_{sc} = 7–10 cm, see Fig. 1b, consisting of material phases with characteristic dimensions d_{sc} = 1–15 mm: (i) cement paste with volume fraction $\bar{f}_{cp}$ and stiffness according to (14), and (ii) aggregates with volume fraction $\bar{f}_{agg} = 1 - \bar{f}_{cp}$ and stiffness according to direct experiments on limestone aggregate (see Table 1). Elasticity homogenization results in a macroscopic law of the form

$$\mathbf{\Sigma}_{sc} = \mathbf{C}_{sc} : \mathbf{E}_{sc} . \tag{21}$$

The homogenization procedure is similar to the one described in (1) – (14). However, there is one fundamental difference: From a morphological viewpoint, the aggregates constitute *inclusions* in a cement paste *matrix* so that choosing a phase stiffness for $\mathbf{C}^0$, namely $\mathbf{C}^0 = \mathbf{C}_{cp}$, is appropriate rather than the choice of the overall RVE$_{sc}$-related stiffness, i.e. $\mathbf{C}^0 \neq \mathbf{C}_{sc}$ (Zaoui, 2002).

Accordingly, the homogenized stiffness of shotcrete is of the Mori–Tanaka form (Mori and Tanaka, 1973; Benveniste, 1987), reading as

$$\mathbf{C}_{sc} = \left\{ \bar{f}_{cp} \mathbf{C}_{cp} + \bar{f}_{agg} \mathbf{C}_{agg} : \left[\mathbf{I} + \mathbf{P}_{sph}^{cp} : (\mathbf{C}_{agg} - \mathbf{C}_{cp}) \right]^{-1} \right\} : : \left\{ \bar{f}_{cp} \mathbf{I} + \bar{f}_{agg} \left[\mathbf{I} + \mathbf{P}_{sph}^{cp} : (\mathbf{C}_{agg} - \mathbf{C}_{cp}) \right]^{-1} \right\}^{-1} . \tag{22}$$

The homogenized strength of shotcrete is obtained analogously to that of cement paste. Thus, σ_{crit}^{dev} is related to the uniaxial compressive strength of shotcrete, $\Sigma_{sc,11}^{comp,ult}$, by the homogenized compliance of shotcrete, $\mathbf{C}_{sc}^{-1}$, obtained from (22),

$$\Sigma_{sc,11}^{comp,ult} = \left\{ \max_{\varphi,\vartheta} \left[\lim_{\Delta\varphi,\Delta\vartheta\to 0} \left(-\frac{\mu_{hyd}^2}{\bar{f}_{hyd;\varphi,\vartheta}} (\mathbf{e}_z \otimes \mathbf{e}_z) : \frac{\partial \mathbf{C}_{sc}^{-1}}{\partial \mu_{hyd;\varphi,\vartheta}} : \right.\right.\right. \\ \left.\left.\left. : (\mathbf{e}_z \otimes \mathbf{e}_z) \right)^{\frac{1}{2}} \right] \right\}^{-1} \times \sigma_{crit}^{dev} . \tag{23}$$

An algorithm for computation of the aforementioned limit, $\lim_{\Delta\varphi,\Delta\vartheta\to 0}$, is presented in Pichler et al. (2008b).

5. Experimental validation of micromechanics-based material models

The micromechanical model presented in Sections 3 and 4, based on the universal phase properties of Table 1, will be fed with shotcrete mixture and hydration kinetics-specific input data concerning material composition, i.e. with experimental values for the volume fractions of air, water, clinker, hydrates, cement paste, and aggregate: f_{air}, f_{H_2O}, f_{clin}, f_{hyd}, $\bar{f}_{cp}$ and $\bar{f}_{agg}$. For these input data, the model delivers predictions for mixture and hydration-specific shotcrete stiffnesses and strengths. Comparison of these predictions to corresponding experimentally derived values allows for assessing the predictive capabilities of the model.

5.1. MIXTURE-DEPENDENT SHOTCRETE COMPOSITION

The volume fractions inside an RVE$_{cp}$ of cement paste depend on the degree of hydration ξ which can be defined as mass of formed hydrates over the mass of hydrates formed if the entire clinker reacts with water, hence $0 \leq \xi \leq 1$. Besides ξ, the w/c-ratio governs the volume fractions f_{air}, f_{H_2O}, f_{clin}, f_{hyd}, so that we consider, according Acker (2001), that

$$f_{clin}(\xi) = \frac{1-\xi}{1 + \dfrac{\rho_{clin}}{\rho_{H_2O}}(w/c)} = \frac{20(1-\xi)}{20 + 63(w/c)} \geq 0 \, , \tag{24}$$

$$f_{H_2O}(\xi) = \frac{\rho_{clin}[(w/c) - 0.42\xi]}{\rho_{H_2O}\left[1 + \dfrac{\rho_{clin}}{\rho_{H_2O}}(w/c)\right]} = \frac{63\,(w/c - 0.42\xi)}{20 + 63(w/c)} \geq 0 \, , \tag{25}$$

$$f_{hyd}(\xi) = \frac{1.42\rho_{clin}\xi}{\rho_{H_2O}\left[1 + \dfrac{\rho_{clin}}{\rho_{H_2O}}(w/c)\right]} = \frac{43.15\xi}{20 + 63(w/c)} \, , \tag{26}$$

$$f_{air}(\xi) = \frac{\left(1 + 0.42\dfrac{\rho_{clin}}{\rho_{H_2O}} - 1.42\dfrac{\rho_{clin}}{\rho_{hyd}}\right)\xi}{1 + \dfrac{\rho_{clin}}{\rho_{H_2O}}(w/c)} = \frac{3.31\xi}{20 + 63(w/c)}\,, \qquad (27)$$

with the mass densities of clinker, water, and hydrates, ρ_{clin}, ρ_{H_2O}, and ρ_{hyd}, following from Acker (2001), see also Pichler et al. (2008a): $\rho_{clin} = 3.15\,\mathrm{kg/dm^3}$, $\rho_{H_2O} = 1\,\mathrm{kg/dm^3}$, and $\rho_{hyd} = 2.073\,\mathrm{kg/dm^3}$. The creation of air voids filling f_{air} stems from the fact that hydration products occupy a smaller volume than their reactants, see e.g. Acker and Ulm (2001). In contrast to the volume fractions within the RVE_{cp}, the volume fractions of cement paste and aggregates do not change during hydration of the material. They can be determined from the water–cement ratio (w/c), the aggregate–cement ratio (a/c), and the mass densities of aggregates, water, and clinker, ρ_{agg}, ρ_{H_2O}, and ρ_{clin} (Acker, 2001; Pichler et al., 2008a), through Bernard et al. (2003)

$$\bar{f}_{agg} = \frac{(a/c)/\rho_{agg}}{1/\rho_{clin} + (w/c)/\rho_{H_2O} + (a/c)/\rho_{agg}} \quad \text{and} \quad \bar{f}_{cp} = 1 - \bar{f}_{agg}\,, \qquad (28)$$

with $\rho_{agg} = 2.5\,\mathrm{kg/dm^3}$. The evolution of the degree of hydration is determined by means of adiabatic tests where the measured accumulated hydration heat is considered as an indicator for the hydration progress of the investigated shotcrete specimen (Ulm and Coussy, 1996; Hellmich, 1999).

5.2. EXPERIMENTAL VALIDATION ON CEMENT PASTE LEVEL

Young's moduli and the compressive strengths of cement paste are estimated by the self-consistent homogenization step depicted in Fig. 1a, for mixture- and hydration degree-specific volume fractions, (24)–(28), on the basis of universal phase stiffnesses (Table 1) and strength values (Section 3.2).

The microelastic model of cement paste is validated by comparing model-predicted to experimentally obtained dynamic Young's moduli and dynamic shear moduli, for w/c-ratios ranging from 0.35 to 0.60 (Sun et al., 2005). The agreement between model predictions and corresponding experimental results, obtained under drained conditions, is satisfactory, see Figs. 3a–c and Pichler et al. (2008a).

By comparing model-predicted to experimentally obtained values for the uniaxial strength of cement pastes with different w/c-ratios, a prediction accuracy, quantified by a squared correlation coefficient $r^2 = 97\%$, is obtained, see Fig. 3d. This corroborates the assumption of the single strength-type value for hydrates, $\sigma_{crit}^{dev} = 26\,\mathrm{MPa}$ (Pichler et al., 2008a).

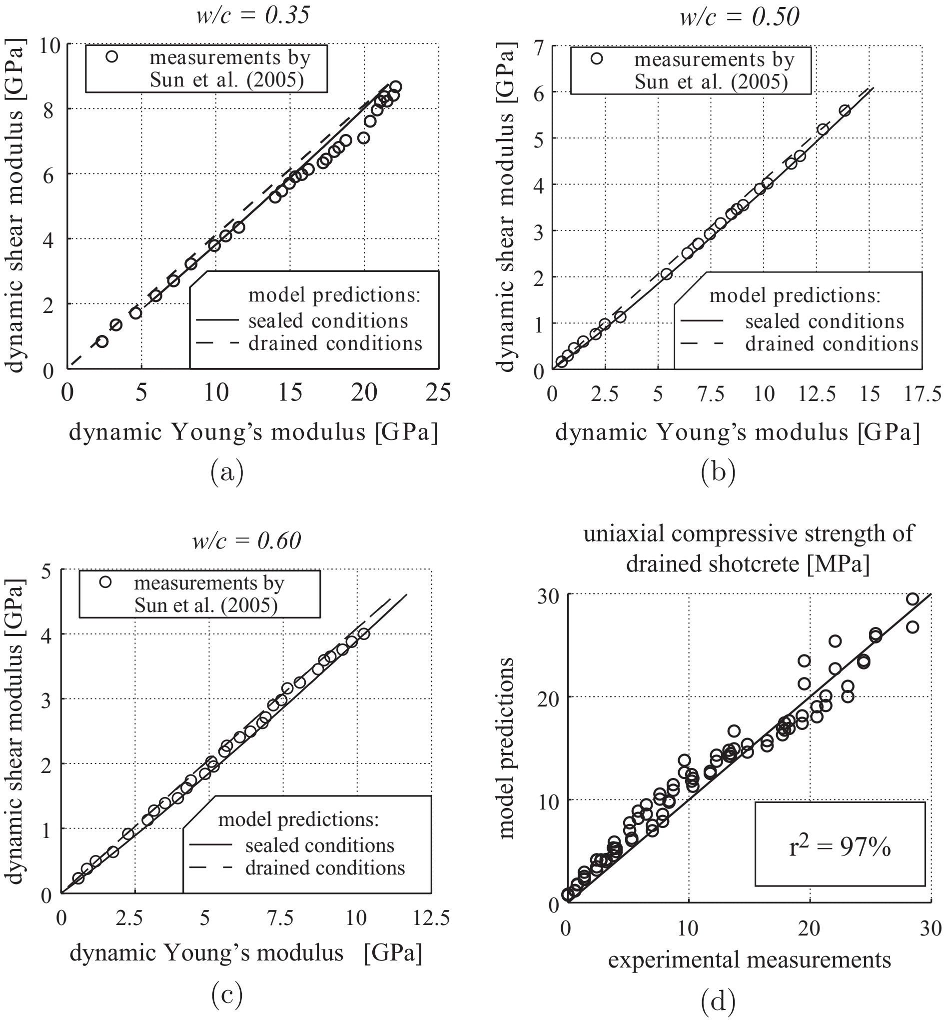

Figure 3. Comparison of model predictions with experimental data characterized by different w/c-ratios ($w/c = 0.35,\ 0.50,\ 0.60$): (**a**–**c**) dynamic shear modulus versus dynamic Young's modulus, and (**d**) uniaxial compressive strength of drained cement paste

5.3. EXPERIMENTAL VALIDATION ON SHOTCRETE LEVEL

A second homogenization step, resulting in a two-step homogenization scheme, is necessary to predict stiffnesses and strengths of shotcrete, see Fig. 1b and Section 4.

For the sake of experimental model validation, the model-predicted Young's modulus of shotcrete is compared to corresponding experimental values of Lafarge (2002) who subjected a shotcrete characterized by $w/c = 0.48$ and $a/c = 5.3$, to resonant frequency tests, see Fig. 4a. The agreement between model predictions and experiments is excellent

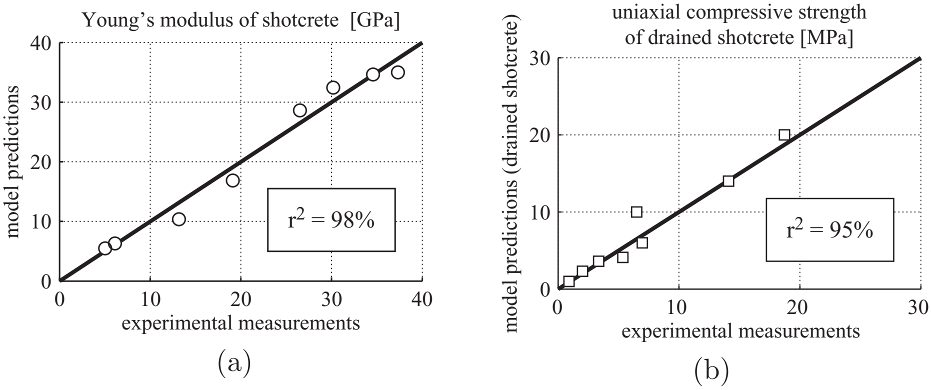

Figure 4. Comparison of model predictions with experimental data characterized by $w/c = 0.48$, $a/c = 5.3$, by $w/c = 0.5$, $a/c = 3.8$, and by $w/c = 0.4$, $a/c = 3.94$, respectively: (**a**) Young's modulus of shotcrete and (**b**) uniaxial compressive strength of drained shotcrete

for sealed conditions (underlined by a mean relative error of 1.0% and a corresponding standard deviation of 6.5%), confirming findings in Hellmich and Mang (2005) that the tests of (Lafarge, 2002) are rather characterized by sealed than by drained conditions. Model predictions related to sealed conditions correlate to experimental results by $r^2 = 98.8\%$, see Fig. 4a.

Experimental validation of the micromechanics-based homogenization of shotcrete strength is carried out according to the experiments of (Lafarge, 1997) and (Pillar, 2002): The applied methodology of experimental strength determination (Hilti gun and penetrometer tests) suggests that model predictions referring to drained conditions are closer to the experimental findings than the ones referring to sealed conditions (Pichler et al., 2008b). The agreement between model predictions (related to drained conditions) and experimental data, characterized by $w/c = 0.5$, $a/c = 3.8$ (Pillar, 2002), and by $w/c = 0.4$, $a/c = 3.94$ (Lafarge, 1997), is quantified by a mean relative prediction error of -5.0% and by a related standard deviation of 19.4%. The relative errors constitute upper bounds (Pichler et al., 2008b), suggesting that the correlation between model predictions and experimental values of $r^2 = 95\%$ is satisfactory, see Fig. 4b.

6. Micromechanics-based shotcrete characterization: influence of water–cement and aggregate–cement ratios on evolutions of elasticity and strength

The experimentally validated micromechanics model (see Sections 3 to 5) allow for predicting hydration degree-dependent evolutions of Young's modulus, Poisson's ratio, and the uniaxial compressive strength of different shotcrete mixtures as functions of their w/c- and a/c-ratios, see Figs. 5 and 6. We observe that Poisson's ratio increases or decreases with

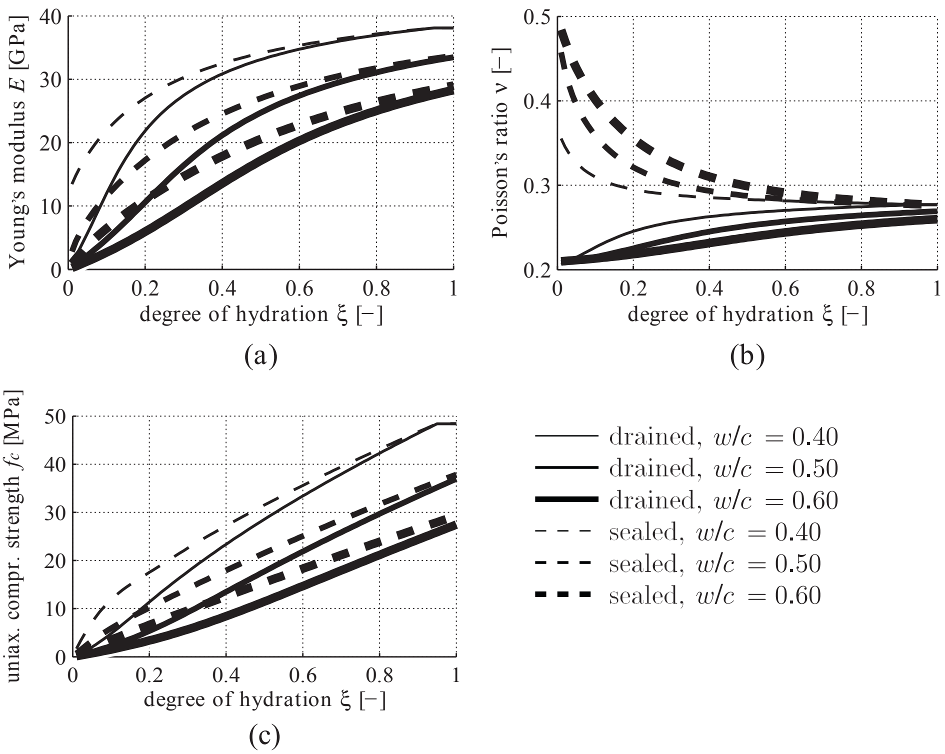

Figure 5. Micromechanics-based input for hybrid analyses of Section 7: Evolutions of (**a**) Young's modulus E, (**b**) Poisson's ratio ν, and (**c**) uniaxial compressive strength f_c, respectively, over the hydration degree ξ; diagrams refer to shotcrete with $a/c = 5$, three different w/c-ratios ($w/c = 0.40,\ 0.50,\ 0.60$), under drained as well as under sealed conditions

increasing water–cement ratio, for drained or sealed conditions, respectively, see Figs. 5b and 6c and d. Sealed conditions, as a rule, lead to higher stiffness and strength values when compared to drained conditions, but this difference becomes very small for complete hydration ($\xi \rightarrow 1$), see Figs. 5 and 6. We also observe that both Young's modulus and the uniaxial compressive

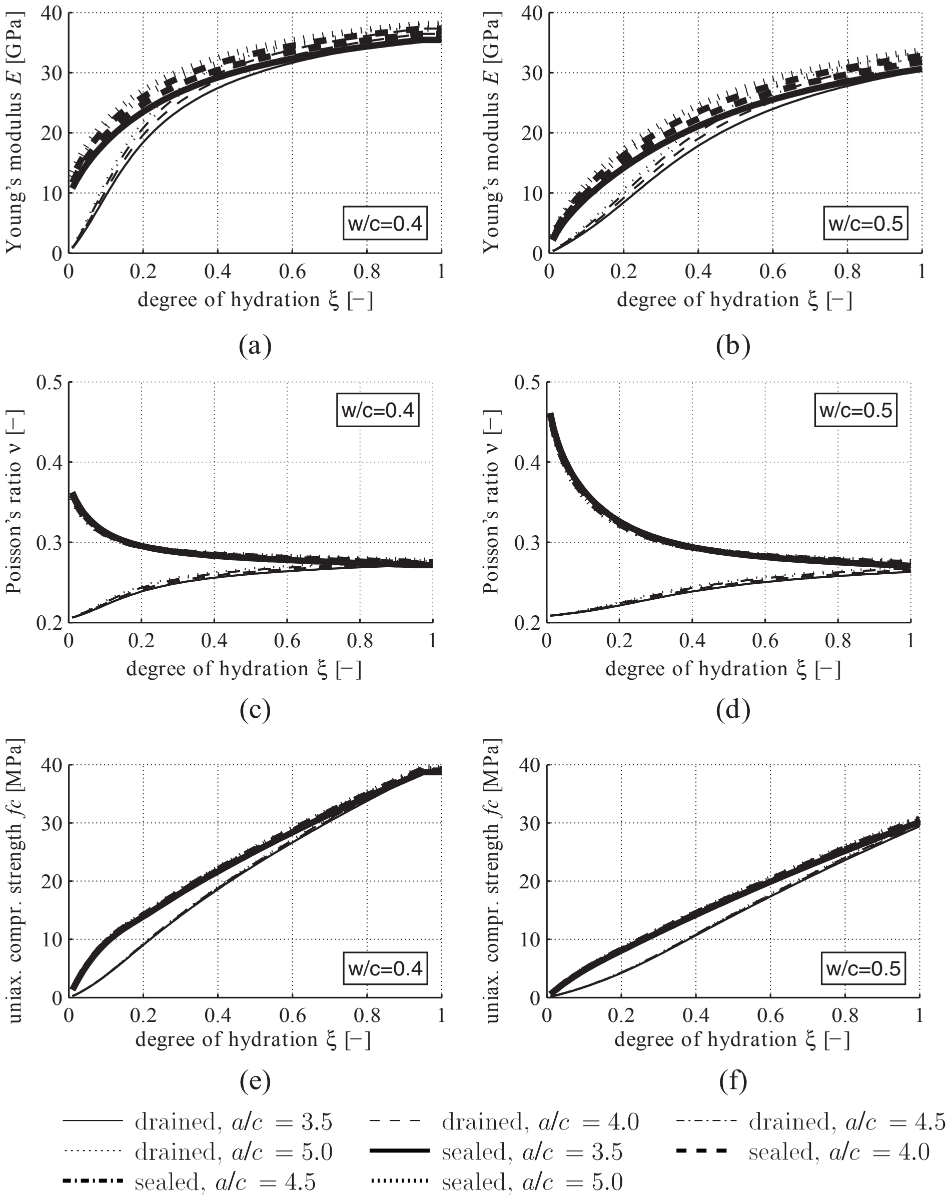

Figure 6. Micromechanics-based input for hybrid analyses of Section 7: Evolutions of (**a**,**b**) Young's modulus E, (**c**,**d**) Poisson's ratio ν, and (**e**,**f**) uniaxial compressive strength f_c, respectively, over the hydration degree ξ; diagrams refer to shotcrete with $w/c = 0.40$ (**a**,**c**,**e**) and $w/c = 0.50$ (**b**,**d**,**f**), four different a/c-ratios ($a/c = 3.5,\ 4.0,\ 4.5,\ 5.0$), under drained as well as under sealed conditions

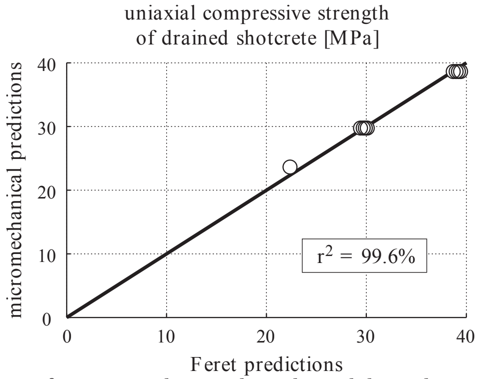

Figure 7. Comparison of micromechanics-based model predictions with predictions of Feret's formula (29) specified for $P = 197.2\,\text{MPa}$

strength decrease with increasing water–cement ratio, whereby the percental decrease of Young's modulus is smaller than that of the compressive strength, see Fig. 5a and c. The loss in final strength (at completed hydration) with increasing water–cement ratio almost perfectly follows Feret's famous empirical relationship (Feret, 1892), stating that the final strength $[\Sigma^{ult}(t = \infty)]$ is proportional to the square of a ratio between the volumes of cement, water, and air contained in a material volume of concrete,

$$\Sigma^{ult}(t = \infty) = P \left[\frac{f_{clin}(\xi = 0)}{f_{clin}(\xi = 0) + f_{H_2O}(\xi = 0) + f_{air}(\xi = 0)} \right]^2 \qquad (29)$$

where P is a factor of proportionality. This relationship has proven remarkable usefulness, and it is widely used for mix designs in the cement and concrete industry: The match between this relationship (with $P = 197.2\,\text{MPa}$) and the model-predicted strength at completed hydration, see Fig. 7, further corroborates the relevance of our model, in addition to the experimental evidence given in Section 5 and in earlier publications Pichler et al. 2008a, b.

Remarkably, Feret's formula (29) does not include the aggregate volume, whereas our model directly accounts for the influence of the aggregate-cement ratio. However, increase of the a/c ratio from 3.5 to 5.0 results in an increase of Young's modulus of only up to 10%, see Fig. 6a and b, whereas Poisson's ratio and the uniaxial compressive strength are virtually unaffected by such variations of the shotcrete mixture, see Fig. 6c–f. It is concluded that for typical shotcretes used in NATM tunneling, the a/c ratio plays a minor role in determining the overall mechanical properties – and this is beneficial to the reliability of structural computations as will be detailed in the next subsection.

7. Continuum micromechanics-based safety assessment of NATM tunnel shells

Finally, the continuum micromechanics-based, hydration degree-dependent evolutions of Young's modulus $E(\xi)$, Poisson's ratio $\nu(\xi)$, and the uniaxial compressive strength $f_c(\xi)$ of shotcrete, given in Section 6, serve as input for the assessment of the degree of utilization of shotcrete tunnel shells by means of the hybrid method according to (Hellmich et al., 2001). This will

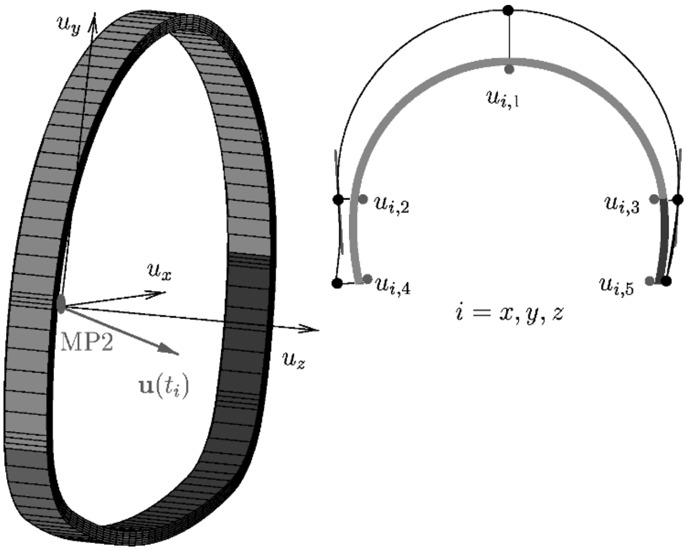

Figure 8. Hybrid method for determination of the level of loading from prescription of measured displacements on a three-dimensional finite element model of the tunnel shell

elucidate the dependence of the structural safety of shotcrete tunnel shells on the shotcrete mixture, governed by the w/c and a/c ratios. Moreover, we examine the role of water with respect to the degree of utilization, by considering both sealed and drained conditions (see Table 1). All other thermochemomechanical phenomena in shotcrete, especially concerning autogeneous shrinkage and creep, are considered macroscopically: In detail, the thermochemomechanical material law proposed by (Hellmich et al., 1999c; Sercombe et al., 2000; Lechner et al., 2001) is employed, considering the relations shown in Fig. 5 for aging elasticity and strength. The remaining material functions (for chemical affinity, creep, and shrinkage) are given in (Lechner et al., 2001), whereby short-term creep is considered according to (Macht et al., 2001).

For simulations based on the hybrid method, displacements measured at km 156.990 of the Sieberg tunnel, in Austria, are prescribed as boundary conditions for a three-dimensional Finite Element model of the tunnel shell as shown in Fig. 8, compare (Hellmich 1999; Hellmich et al., 1999a, 2001). Simulation results are illustrated in terms of the so-called level of loading $\mathscr{L}$ which can be interpreted as the degree of utilization. The latter is defined as the ratio of the loading (stress) over loading capacity (strength) of the shotcrete tunnel shell. More specifically, it is defined on the basis of a Drucker-Prager failure surface calibrated for uniaxial and biaxial compressive failure, $\Sigma_{sc,11}^{comp,ult}$ from (23), and $\Sigma_{sc,11}^{Bicomp,ult} = \Sigma_{sc,11}^{comp,ult} \times \kappa$, with $\kappa = 1.16 = \text{constant}$,

$$\mathscr{L} = \frac{\alpha \mathrm{tr}\, \mathbf{\Sigma}_{sc} + \sqrt{\Sigma_{sc,ij}^{dev} \Sigma_{sc,ij}^{dev}}}{k} \tag{30}$$

with

$$\alpha = \sqrt{\frac{2}{3}} \frac{\kappa - 1}{2\kappa - 1}, \quad k = \sqrt{\frac{2}{3}} \left(1 - \frac{\kappa - 1}{2\kappa - 1}\right) \Sigma_{sc,11}^{comp,ult} \tag{31}$$

In the present evaluation we focus on the average nature of $\mathscr{L}$ over the tunnel shell thickness h,

$$\overline{\mathscr{L}}(\varphi, t) = \frac{1}{h} \int_h \mathscr{L}(r, \varphi, t)\, dr\,, \tag{32}$$

with r and φ as polar coordinates defining (macroscopic) positions within a circular shell segment, and we designate the maximum value of $\overline{\mathscr{L}}(\varphi, t)$ in the tunnel shell, $\overline{\mathscr{L}}_{max}(t)$, as the 'level of loading' in Fig. 9a and b.

7.1. WATER–CEMENT RATIO-DEPENDENCE OF STRUCTURAL SAFETY

Three shotcrete mixtures are investigated: $w/c = 0.40$ (mix I), $w/c = 0.50$ (mix II), and $w/c = 0.60$ (mix III), each with $a/c = 5$, see Fig. 5. The simulation results show that throughout the observed loading phase the resulting level of loading of the tunnel shell is decisively influenced by the w/c-ratio, see Fig. 8b and c. In detail, the level of loading for $w/c = 0.40$ is around 40% lower than the one for $w/c = 0.60$. At the end of the observed loading phase, 1,120 h after installation of the top heading, simulations based on $w/c = 0.60$ predict a level of loading reaching 100% which would indicate severe cracking or even failure of the tunnel shell, whereas for both $w/c = 0.40$ and $w/c = 0.50$ the tunnel shell is intact, see Fig. 8b and c. The significant increase of the level of loading in the tunnel shell with increasing w/c-ratio can be explained as follows: With increasing water–cement ratio the percental decrease in macroscopic stiffness (e.g. Young's modulus) of shotcrete is smaller than the percental decrease in the uniaxial compressive strength of the material, see Fig. 5a and c. Whereas a slightly reduced elastic

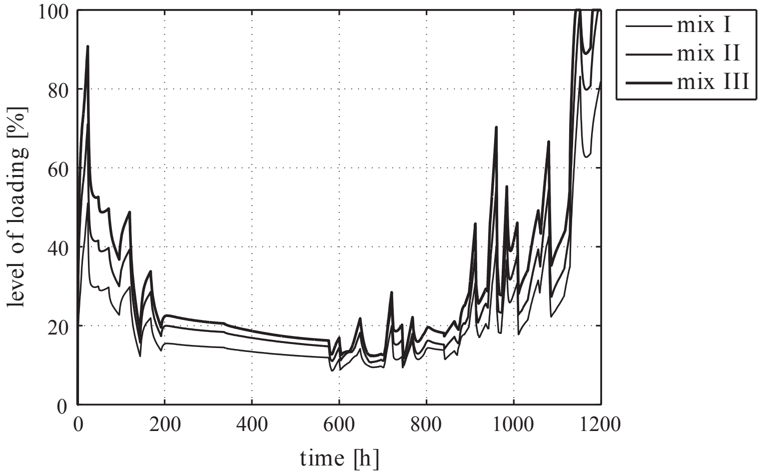

(a) sealed conditions

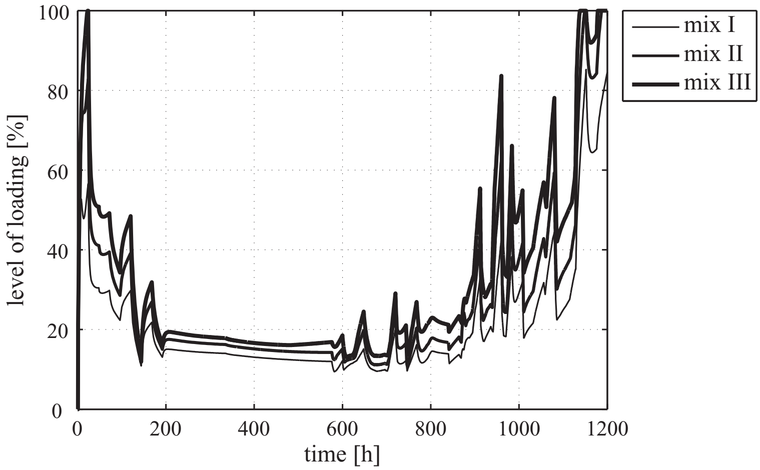

(b) drained conditions

Figure 9. Evolution of the level of loading $\overline{\mathscr{L}}_{max}$ as function of the time after installation of the top heading for (**a**) sealed conditions, and (**b**) drained conditions, determined through hybrid analyses

stiffness activates only slightly smaller forces within the shotcrete tunnel shell, a more pronounced loss in uniaxial compressive strength significantly reduces the load-carrying capacity of the material. Hence, the larger the water–cement ratio, the smaller the material resistance, and the reduced load-carrying capacity cannot be compensated by smaller forces in the tunnel shell caused by the reduced stiffness of the material. It is concluded that rather small water–cement ratios (that is, high cement contents) are beneficial to shotcrete tunnel shells. This further motivates the development of additives which reduce water contents typically encountered in real-life applications. On the other hand, the deviations between the levels of loading predicted for sealed conditions in the shotcrete, see Fig. 8b, only negligibly differ from those predicted for drained conditions in the shotcrete, see Fig. 8c. Still, we note that, in principal, sealed conditions result in slightly lower levels of loading as compared to drained conditions.

7.2. AGGREGATE–CEMENT RATIO-DEPENDENCE OF STRUCTURAL SAFETY

During shotcreting, shotcrete constituents may detach from the sprayed material, which is referred to as rebound. Assuming rebound to concern aggregates only (m_{clin} = const., m_{H_2O} = const.), the a/c ratio decreases with respect to the targeted a/c ratio, denoted as $(a/c)_{target}$, namely: $a/c = (a/c)_{target} - \Delta(a/c)_{rebound}$. Considering that the targeted mass of shotcrete, $m_{sc,target}$, is composed of the mass of clinker, water, and aggregates,

$$m_{sc,target} = m_{clin} + m_{H_2O} + m_{agg} = m_{clin}\left(1 + w/c + (a/c)_{target}\right) , \quad (33)$$

and that the shotcrete mass remaining on the tunnel wall, m_{sc}, is related to $m_{sc,target}$ by rebound R,

$$m_{sc} = m_{sc,target}(1 - R) = m_{clin}\left(1 + w/c + a/c\right) , \quad (34)$$

allows, through substitution of (33) into (34), for estimation of the actual a/c ratio as a function of the rebound R, the water–cement ratio w/c, and the targeted aggregate–cement ratio $(a/c)_{target}$,

$$a/c = (a/c)_{target} - R\left(1 + w/c + (a/c)_{target}\right) . \quad (35)$$

For wet shotcreting, as has been used in the Sieberg tunnel, the rebound hardly exceeds 20% (Hague, 2001).[1] In order to elucidate the dependence of the structural safety on rebound-related variations of the a/c-ratio, eight different mixes are investigated (see Table 2 for corresponding rebounds as $(a/c)_{target} = 5.0$): $w/c = 0.40$ and $a/c = 3.5$ (mix IV), $w/c = 0.40$ and $a/c = 4.0$ (mix V), $w/c = 0.40$ and $a/c = 4.5$ (mix VI), $w/c = 0.40$ and $a/c = 5.0$ (mix VII), $w/c = 0.50$ and $a/c = 3.5$ (mix VIII), $w/c = 0.50$ and $a/c = 4.0$ (mix IX), $w/c = 0.50$ and $a/c = 4.5$ (mix X), as well as $w/c = 0.50$ and $a/c = 5.0$ (mix XI), see Fig. 6 for the micromechanics-based material properties.

[1] Dry shotcreting may lead to higher rebounds (Armelin and Banthia, 1998; Pfeuffer and Kusterle, 2001).

TABLE 2. Shotcrete rebound R for given values of w/c and a/c; according to (35); for $(a/c)_{target} = 5.0$

a/c	$w/c = 0.40$	$w/c = 0.50$
5.0	$R = 0.0\%$	$R = 0.0\%$
4.5	$R = 7.8\%$	$R = 7.7\%$
4.0	$R = 15.6\%$	$R = 15.4\%$
3.5	$R = 23.4\%$	$R = 23.1\%$

In contrast to the w/c ratio, the (effective) a/c ratio has no significant influence on the level of loading of the shotcrete tunnel shell, see Fig. 10. This is because the a/c ratio increase-related increase of Young's modulus (see Fig. 6), letting expect higher utilization degrees in the tunnel shell, is compensated by stress redistributions in the tunnel shell. Hence, the level of loading shows no significant dependence on the (actual) a/c ratio for the investigated shotcrete mixtures. This structural behavior can be considered as beneficial: Our calculations suggest that such changes of the (actual) a/c ratio because of shotcrete rebound do not compromise the structural safety of the tunnel shell. Since the investigated shotcrete mixes exhibit a maximum rebound of 23.4% (see Table 2), thus comprising common rebounds in wet shotcreting, the insensitity of the loading level of the tunnel shell with respect to aggregate rebound is a robust feature of the NATM. It suggests that careful *in situ* monitoring of the w/c ratio, as compared to the a/c ratio, is much more critical.

8. Conclusions

We have developed a new micromechanics model which economically accounts for the impact of the shotcrete composition on the elasticity and strength properties of the material. On this basis, we have shown the potentially major influence of the shotcrete composition (in particular of the water–cement ratio) on the forces induced in a NATM-tunnel shell. To further elucidate this role, it is highly desirable to extend the micromechanical description of shotcrete towards consideration of both creep and shrinkage. This is a topic of ongoing research. Another open issue relates to the question whether high levels of loading (such as those encountered in Figs. 8b and c 1,120 h after shell installation) might be overestimations as a result of enforcing $C1$-continuity of displacements between shell components

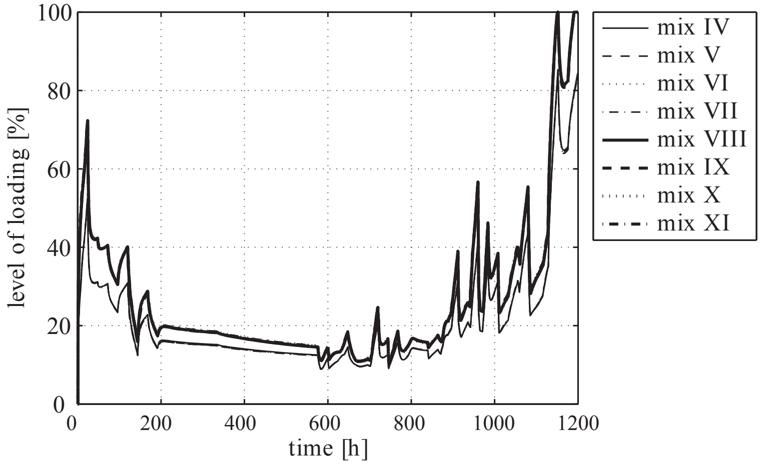

(a) sealed conditions

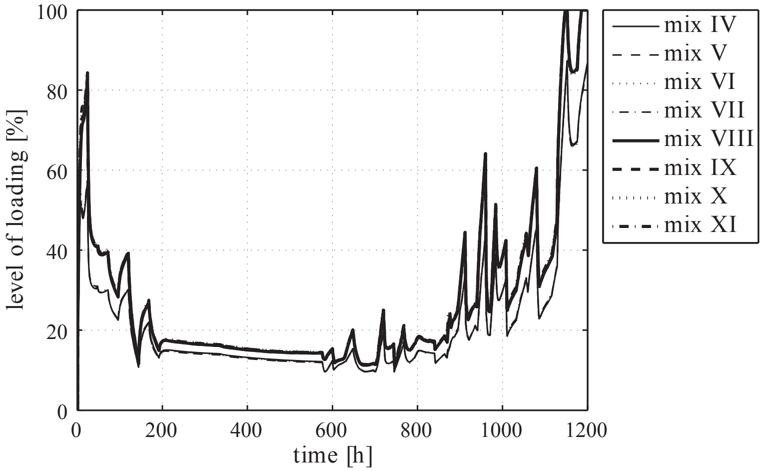

(b) drained conditions

Figure 10. Evolution of the level of loading $\overline{\mathscr{L}}_{max}$ as function of the time after installation of the top heading for (**a**) sealed conditions, and (**b**) drained conditions, determined through hybrid analyses

installed at different time instants, see (Hellmich et al., 1999a, 2001) for details. This underlines that further improvement of data analysis during NATM-tunneling calls for even more refined applied mechanics tools, both at the material level (microstructural level = shotcrete) and at the (macro-) structure level (= tunnel shell).

Acknowledgements

This work was part of the micromechanics-based activities within the integrated project ‘Technology Innovation in Underground Construction – TUNCONSTUCT’ (http://www.tunconstruct.org), co-sponsored by the European Commission.

References

Acker, P. (2001). Micromechanical analysis of creep and shrinkage mechanisms. In Ulm, F.-J., Bažant, Z., and Wittmann, F., editors, *Creep, shrinkage and durability mechanics of concrete and other quasi-brittle materials*, 6th International Conference CONCREEP@MIT, pages 15–26, Amsterdam: Elsevier.

Acker, P. and Ulm, F.-J. (2001). Creep and shrinkage of concrete: physical origins and practical measurements. *Nuclear Engineering and Design*, 203(2–3):143–158.

Armelin, H. and Banthia, N. (1998). Development of a general model of aggregate rebound for dry-mix shotcrete (Part II). *Materials and Structures*, 31(207):195–202.

Baroghel-Bouny, V. (1994). Caractérisation des pâtes de ciment et des bétons-méthodes, analyse, interprétation [Characterization of cement pastes and concretes-methods, analysis, interpretations]. Technical report, Laboratoire Central des Ponts et Chaussées, Paris, France. In French.

Barthélémy, J.-F. and Dormieux, L. (2003). Détermination du critère de rupture macroscopique d’un milieu poreux par homogénéisation non linèaire [Determination of the macroscopic strength criterion of a porous medium by nonlinear homogenization]. *Comptes Rendus Mécanique*, 331(4):271–276. In French.

Beer, G. (2003). *Numerical Simulation in Tunneling*. Springer Verlag Wien New York.

Benveniste, Y. (1987). A new approach to the application of Mori–Tanaka’s theory in composite materials. *Mechanics of Materials*, 6(2):147–157.

Bernard, O., Ulm, F.-J., and Lemarchand, E. (2003). A multiscale micromechanics-hydration model for the early-age elastic properties of cement-based materials. *Cement and Concrete Research*, 33(9):1293–1309.

Bishop, P. (1994). Industry hit by Heathrow implications. *New Civil Engineer*, 27:3.

Boumiz, A., Vernet, C., and Cohen-Tenoudji, F. (1996). Mechanical properties of cement pastes and mortars at early ages. *Advanced Cement Based Materials*, 3(3–4):94–106.

Brandtner, P., Moritz, B., and Schubert, P. (2007). On the challenge of evaluating stress in a shotcrete lining: Experiences gained in applying the hybrid analysis method. *Felsbau*, 25(5):93–98.

Constantinides, G. and Ulm, F.-J. (2004). The effect of two types of C-S-H on the elasticity of cement-based materials: Results from nanoindentation and micromechanical modeling. *Cement and Concrete Research*, 34(1):67–80.

Dormieux, L., Molinari, A., and Kondo, D. (2002). Micromechanical approach to the behavior of poroelastic materials. *Journal of Mechanics and Physics of Solids*, 50(10):2203–2231.

Dormieux, L., Sanahuja, J., and Maalej, Y. (2007). Résistance d’un polycristal avec interfaces intergranulaires imparfaites [Strength of a polycrystal with imperfect intergranular interfaces]. *Comptes Rendus Mecanique*, 335(1):25–31. In French.

Eshelby, J. (1957). The determination of the elastic field of an ellipsoidal inclusion, and related problems. *Proceedings of the Royal Society of London A*, 241:376–396. Reprinted in Markenscoff and Gupta (2006).

Feret, R. (1892). On the compactness of hydraulic mortars [Sur la compacitée des mortiers hydrauliques]. *Annales des Ponts et Chaussées*, 7:5–164. In French.

Fritsch, A., Dormieux, L., Hellmich, C., and Sanahuja, J. (2007). Micromechanics of crystal interfaces in polycrystalline solid phases of porous media: Fundamentals and application to strength of hydroxyapatite biomaterials. *Journal of Materials Science*, 42(21):8824–8837.

Hague, I. (2001). Wet shotcreting – A total system approach. *www.ugc.basf.com* (last download: July 31, 2008).

Hashin, Z. (1983). Analysis of composite materials – A survey. *Journal of Applied Mechanics*, 50(3):481–505.

Hellmich, C. (1999). *Shotcrete as part of the New Austrian tunneling method: From thermochemomechanical material modeling to structural analysis and safety assessment of tunnels*. Ph.D. thesis, Vienna University of Technology, Vienna, Austria.

Hellmich, C. and Ulm, F.-J. (2002). Micromechanical model for ultra-structural stiffness of mineralized tissues. *Journal of Engineering Mechanics (ASCE)*, 128(8):898–908.

Hellmich, C. and Ulm, F.-J. (2005). Drained and undrained poroelastic properties of healthy and pathological bone: A poro-micromechanical investigation. *Transport in Porous Media*, 58(3):243–268.

Hellmich, C., Macht, J., and Mang, H. (1999a). Ein hybrides Verfahren zur Bestimmung der Auslastung von Spritzbetonschalen [A hybrid method for determination of the level of utilization of shotcrete shells]. *Felsbau*, 17(5):422–425. In German.

Hellmich, C., Ulm, F.-J., and Mang, H. (1999b). Consistent linearization in finite element analysis of coupled chemo-thermal problems with exo- or endothermal reactions. *Computational Mechanics*, 24(4):238–244.

Hellmich, C., Ulm, F.-J., and Mang, H. (1999c). Multisurface chemoplasticity I: Material model for shotcrete. *Journal of Engineering Mechanics (ASCE)*, 125(6):692–701.

Hellmich, C., Mang, H., and Ulm, F.-J. (2001). Hybrid method for quantification of stress states in shotcrete tunnel shells: Combination of 3D in situ displacement measurements and thermochemoplastic material law. *Computers and Structures*, 79(22–25):2103–2115.

Hellmich, C. and Mang, H. (2005). Shotcrete elasticity revisited in the framework of continuum micromechanics: From submicron to meter level. *Journal of Materials in Civil Engineering (ASCE)*, 17(3):246–256.

Hershey, A. (1954). The elasticity of an isotropic aggregate of anisotropic cubic crystals. *Journal of Applied Mechanics (ASME)*, 21:226–240.

Hill, R. (1963). Elastic properties of reinforced solids. *Journal of the Mechanics and Physics of Solids*, 11(5):357–372.

Hofstetter, K., Hellmich, C., and Eberhardsteiner, J. (2005). Predicting wood strength from composition and microstructure: Development and experimental verification of a continuum micromechanics model. In Dormieux, L., Kondo, D., and Sab, K., editors, *Colloque en l'honneur du Professeur Jean-Louis Auriault: Microstructure et Propriétés des Matériaux*, pages 217–222. Presses de l'Ecole Nationale des Ponts et Chaussées.

Karakuş, M. and Fowell, R. (2004). An insight into the new Austrian Tunnelling Method (NATM). In *Rockmec'2004 – VIIth Regional Rock Mechanics Symposium*. Sivas, Turkey.

Kreher, W. (1990). Residual stresses and stored elastic energy of composites and polycrystals. *Journal of the Mechanics and Physics of Solids*, 38(1):115–128.

Kreher, W. and Molinari, A. (1993). Residual stresses in polycrystals as influenced by grain shape and texture. *Journal of the Mechanics and Physics of Solids*, 41(12): 1955–1977.

Kröner, E. (1958). Berechnung der elastischen Konstanten des Vielkristalls aus den Konstanten des Einkristalls [Computation of the elastic constants of a polycrystal based on the constants of the single crystal]. *Zeitschrift für Physik A Hadrons and Nuclei*, 151(4):504–518. In German.

Lackner, R., Macht, J., Hellmich, C., and Mang, H. (2002). Hybrid method for analysis of segmented shotcrete tunnel linings. *Journal of Geotechnical and Geoenvironmental Engineering (ASCE)*, 128(4):298–308.

Lackner, R., Macht, J., and Mang, H. (2006). Hybrid analysis method for on-line quantification of stress states in tunnel shells. *Computer Methods in Applied Mechanics and Engineering*, 195(41–43):5361–5378.

Lafarge (1997). Internal report, Lafarge Centre Technique Europe Central. Commissioned by the Institute for Strength of Materials, Vienna University of Technology, Austria.

Lafarge (2002). Internal report, Lafarge Centre Technique Europe Central. Commissioned by the Institute for Strength of Materials, Vienna University of Technology, Austria.

Laws, N. (1977). The determination of stress and strain concentrations at an ellipsoidal inclusion in an anisotropic material. *Journal of Elasticity*, 7(1):91–97.

Lechner, M., Hellmich, C., and Mang, H. (2001). Short-term creep of shotcrete – Thermochemoplastic material modelling and nonlinear analysis of a laboratory test and of a NATM excavation by the finite element method. In Vermeer, P., Diebels, S., Ehlers, W., Herrmann, H., Luding, S., and Ramm, E., editors, *Proceedings of the International Symposium on Discontinuous Modelling of Cohesive-Frictional Materials – Lecture Notes in Physics*, pages 47–62. Berlin: Springer.

Lemarchand, E., Ulm, F.-J., and Dormieux, L. (2002). Effect of inclusions on friction coefficient of highly filled composite materials. *Journal of Engineering Mechanics (ASCE)*, 128(8):876–884.

Macht, J., Hellmich, C., Lackner, R., Schubert, W., and Mang, H. (2000). Assessment of a support system for squeezing rock conditions by means of a hybrid method. *Felsbau*, 18(6):9–15.

Macht, J., Lackner, R., Hellmich, C., and Mang, H. (2001). Shotcrete creep properties – Review of material tests and structural analyses of tunnels. In Ulm, F.-J., Bažant, Z., and Wittmann, F., editors, *Proceedings of the 6th International Conference on Creep, Shrinkage and Durability Mechanics of Concrete and Other Quasi-brittle Materials*, pages 285–300. Amsterdam: Elsevier.

Macht, J., Lackner, R., Hellmich, C., and Mang, H. (2003). *Quantification of stress states in shotcrete shells*, chapter 10, pages 225–248, Wien New York: Springer. In Beer (2003).

Markenscoff, X. and Gupta, A., editors (2006). *Collected works of J. D. Eshelby – The mechanics of defects and inhomogeneities*, volume 133 of *Solid mechanics and its applications*. Springer. Dordrecht, The Netherlands.

Mehlhorn, G. (1996). *Der ingenieurbau: Grundwissen – Werkstoffe, elastizitätstheorie [Basic knowledge in civil engineering: Materials and elasticity theory]*, volume 4, Berlin: Ernst & Sohn. In German.

Mori, T. and Tanaka, K. (1973). Average stress in matrix and average elastic energy of materials with misfitting inclusions. *Acta Metallurgica*, 21:571–574.

Neville, A. (1981). *Properties of concrete*, Pitman, 3rd edition. London, United Kingdom.
Oliver, A. (1994). Heathrow trial runs under question. *New Civil Engineer*, 3:4.
Pfeuffer, M. and Kusterle, W. (2001). Rheology and rebound behaviour of dry-mix shotcrete. *Cement and Concrete Research*, 31(11):1619–1625.
Pichler, B., Hellmich, C., and Eberhardsteiner, J. (2009). Spherical and acicular representation of hydrates in a micromechanical model for cement paste – Prediction of early-age elasticity and strength. *Acta Mechanica,* 203(3-4):137–162.
Pichler, B., Scheiner, S., and Hellmich, C. (2008). From micron-sized needle-shaped hydrates to meter-sized shotcrete tunnel shells: Micromechanical upscaling of stiffness and strength of hydrating shotcrete. *Acta Geotechinca,* 3(4):273–294.
Pillar, N. (2002). *Determination of early age properties of fibre reinforced shotcrete to predict the cracking behavior*. Ph.D. thesis, submitted to the University of New South Wales, Private Communication, Sydney, Australia.
Rabcewicz, L. (1948). Patentschrift. Österreichisches Patent Nr. 165573 [Patent specification, Austrian patent no. 165573]. In German.
Rabcewicz, L. (1964a). The New Austrian Tunnelling Method, Part one. *Water Power*, pages 453–457.
Rabcewicz, L. (1964b). The New Austrian Tunnelling Method, Part two. *Water Power*, pages 511–515.
Rabcewicz, L. (1965). The New Austrian Tunnelling Method, Part three. *Water Power*, pages 19–24.
Rokahr, R. and Lux, K. (1987). Einfluß des rheologischen Verhaltens des Spritzbetons auf den Ausbauwiderstand [Influence of the rheological behavior of shotcrete on the excavation resistance]. *Felsbau*, 5:11–18.
Rokahr, R. and Zachow, R. (1997). Ein neues Verfahren zur täglichen Kontrolle der Auslastung einer Spritzbetonschale [A new method for daily monitoring of the stress intensity of a sprayed concrete lining]. *Felsbau*, 15(6):430–434. In German.
Schubert, P. (1988). Beitrag zum rheologischen Verhalten von Spritzbeton [Contribution to the rheological behavior of shotcrete]. *Felsbau*, 6:150–153.
Schubert, W. and Steindorfer, A. (1996). Selective displacement monitoring during tunnel excavation. *Felsbau*, 14(2):93–97.
Schubert, W., Steindorfer, A., and Button, E. (2002). Displacement monitoring in tunnels – An overview. *Felsbau*, 20(2):7–15.
Sercombe, J., Hellmich, C., Ulm, F.-J., and Mang, H. (2000). Modeling of early-age creep of shotcrete I: Model and model parameters. *Journal of Engineering Mechanics (ASCE)*, 126(3):284–291.
Steindorfer, A., Schubert, W., and Rabensteiner, K. (1995). Problemorientierte Auswertung geotechnischer Messungen [Advanced evaluation of geotechnical displacement monitoring data]. *Felsbau*, 13(6):386–390. In German.
Sun, Z., Ye, G., and Shah, S. (2005). Microstructure and early-age properties of Portland cement paste: Effects of connectivity of solid phases. *ACI Materials Journal*, 102(1):122–129.
Suquet, P. (1997). *Continuum micromechanics*, volume 377 of *CISM Courses and Lectures*, Wien New York: Springer.
Tritthart, J. and Häußler, F. (2003). Pore solution analysis of cement pastes and nanostructural investigations of hydrated C_3S. *Cement and Concrete Research*, 33(7):1063–1070.

Ulm, F.-J. and Coussy, O. (1996). Strength growth as chemo-plastic hardening in early age concrete. *Journal of Engineering Mechanics (ASCE)*, 122(12):1123–1132.

Ulm, F.-J., Constantinides, G., and Heukamp, F. (2004). Is concrete a poromechanics material? – A multiscale investigation of poroelastic properties. *Materials and Structures/Materiaux et Constructions*, 37(1):43–58.

Wesche, K. (1974). *Baustoffe für tragende Bauteile [Building materials for structural components]*. Bauverlag, Wiesbaden, Germany, 3rd edition. In German.

Zaoui, A. (1997). Structural morphology and constitutive behavior of microheterogeneous materials. In Suquet, P., editor, *Continuum Micromechanics*, pages 291–347, Vienna: Springer.

Zaoui, A. (2002). Continuum micromechanics: Survey. *Journal of Engineering Mechanics (ASCE)*, 128(8):808–816.